Inorganic Chemistry
Article

Inorg. Chem. **2011**, *50*, 757–763 **757**
DOI: 10.1021/ic1017664

Facile Electrochemical Synthesis of Hexagonal Cu_2O Nanotube Arrays and Their Application

Jin-Hui Zhong, Gao-Ren Li,* Zi-Long Wang, Yan-Nan Ou, and Ye-Xiang Tong

MOE Laboratory of Bioinorganic and Synthetic Chemistry, School of Chemistry and Chemical Engineering, Institute of Optoelectronic and Functional Composite Materials, Sun Yat-sen University, Guangzhou 510275, China

Received March 18, 2010

Large-scale and highly oriented single-crystalline hexagonal Cu_2O nanotube arrays have been successfully synthesized using a two-step solution approach, which involves the electrodeposition of oriented Cu_2O nanorods and a subsequent dissolution technique along the *c* axis to form a tubular structure. Herein, NH_4Cl was found to be an effectual additive, and it can successfully realize the dissolution process of Cu_2O from nanorods to nanotubes. The dissolution mechanism of Cu_2O from nanorods to nanotubes was illustrated in detail. These prepared Cu_2O nanotube arrays were characterized by SEM, EDS, XRD, XPS, and TEM. The photoluminescence (PL) spectrum of Cu_2O nanotube arrays was also measured, and it shows there is a greater fraction of copper or oxygen vacancies in these prepared Cu_2O nanotubes. Finally, the applications of Cu_2O nanotube arrays for gas sensors were investigated in this paper.

Introduction

Tubular structured nanomaterials have been greatly explored owing to their fascinating physicochemical properties since the discovery of carbon nanotubes in 1991, and many potential applications have been found, such as their use in nanodevices, catalysis, biomimetics, sensors, and energy storage.[1] Various methods have been developed for the synthesis of nanotubes, such as catalytic pyrolysis, high-temperature evaporation, hydrothermal synthesis, colloidal growth, anodic oxidation, chemical bath deposition, and template- and surfactant-assisted growth techniques.[2−6] However, the synthesis of some kinds of nanotubes such as Cu_2O nanotubes are still restricted by the above methods, although they are very useful. Therefore, some novel synthesis routes still need to be further investigated for the preparation of the special kinds of nanotubes.

Cu_2O, a p-type semiconductor with a direct band gap of about 2.17 eV, has been widely employed in gas sensors,[7] catalysts,[8] solar energy conversion,[9] biosensors,[10] and magnetic storage devices.[11] Cu_2O crystals also have been at the center of research on the Bose−Einstein condensation of excitons.[12] Furthermore, Cu_2O is inexpensive, plentiful, and readily available, with low toxicity and good environmental acceptability, which favors the fundamental and practical research on Cu_2O.[13−15] As size and morphology have strong

*To whom correspondence should be addressed. E-mail: ligaoren@mail.sysu.edu.cn.

(1) Schnur, J. M. *Science* **1993**, *262*, 1669–1676.
(2) Wang, Z. L.; Gao, R. P. P.; Gole, J. L.; Stout, J. D. *Adv. Mater.* **2000**, *12*, 1938–1940.
(3) Hollingsworth, J. A.; Poojary, D. M.; Clearfield, A.; Buhro, W. E. *J. Am. Chem. Soc.* **2000**, *122*, 3562–3563.
(4) Jian, Y.; Wu, Y.; Zhang, S. Y.; Xu, C. Y.; Yu, W. C.; Xie, Y.; Qian, Y. T. *J. Am. Chem. Soc.* **2000**, *122*, 12383–12384.
(5) Li, Y.; Wang, J.; Deng, Z.; Wu, Y.; Sun, X.; Yu, D.; Yang, P. *J. Am. Chem. Soc.* **2001**, *123*, 9904–9905.
(6) Mulvihill, M. J.; Rupert, B. L.; He, R.; Hochbaum, A.; Arnold, J.; Yang, P. *J. Am. Chem. Soc.* **2005**, *127*, 16040–16041.
(7) Zhang, J. T.; Liu, J. F.; Li, Y. D. *Chem. Mater.* **2006**, *18*, 867–871.
(8) (a) Hara, M.; Kondo, T.; Komoda, M.; Ikeda, S.; Shinohara, K.; Tanaka, A.; Kondo, J. N.; Domen, K. *Chem. Commun.* **1998**, 357. (b) De Jongh, P. E.; Vanmaelkelbergh, D.; Kelly, J. J. *Chem. Commun.* **1999**, *12*, 1069–1070. (c) White, B.; Yin, M.; Hall, A.; Le, D.; Stolbov, S.; Rahman, T.; Turro, N.; O'Brien, S. *Nano Lett.* **2006**, *6*, 2095–2098.
(9) (a) McShane, C. M.; Choi, K.-S. *J. Am. Chem. Soc.* **2009**, *131*, 2561–2569. (b) Walker, A. V.; Yates, J. T., Jr. *J. Phys. Chem. B* **2000**, *104*, 9038–9043.
(10) Zhu, H.; Wang, J.; Xu, G. *Crys. Growth Des.* **2009**, *9*, 633–638.
(11) Fishman, D.; Faugeras, C.; Potemski, M.; Revcolevschi, A.; van Loosdrecht, P. H. M. *Phys. Rev. B* **2009**, *80*, 045208.
(12) Snoke, D. *Science* **2002**, *298*, 1368–1372.
(13) (a) Switzer, J. A.; Hung, C.-J.; Huang, L.-Y.; Switzer, E. R.; Kammler, D. R.; Golden, T. D.; Bohannan, E. W. *J. Am. Chem. Soc.* **1998**, *120*, 3530–3531. (b) Bohannan, E. W.; Shumsky, M. G.; Switzer, J. A. *Chem. Mater.* **1999**, *11*, 2289–2291. (c) Golden, T. D.; Shumsky, M. G.; Zhou, Y.; VanderWerf, R. A.; Van Leeuw-en, R. A.; Switzer, J. A. *Chem. Mater.* **1996**, *8*, 2499–2504. (d) Liu, R.; Kulp, E. A.; Oba, F.; Bohannan, E. W.; Ernst, F.; Switzer, J. A. *Chem. Mater.* **2005**, *17*, 725–729.
(14) (a) Barton, J. K.; Vertegel, A. A.; Bohannan, E. W.; Switzer, J. A. *Chem. Mater.* **2001**, *13*, 952–959. (b) Jongh, P. E.; Vanmaekelbergh, D.; Kelly, J. J. *Chem. Mater.* **1999**, *11*, 3512–3517. (c) Zhao, H. Y.; Wang, Y. F.; Zeng, J. H. *Cryst. Growth Des.* **2008**, *8*, 3731–3734. (d) Li, J.; Shi, Y.; Cai, Q.; Sun, Q.; Li, H.; Chen, X.; Wang, X.; Yan, Y.; Vrieling, E. G. *Cryst. Growth Des.* **2008**, *8*, 2652–2659.
(15) (a) Bao, H.; Zhang, W.; Shang, D.; Hua, Q.; Ma, Y.; Jiang, Z.; Yang, J.; Huang, W. *J. Phys. Chem. C* **2010**, *114*, 6676–6680. (b) Li, X.; Gao, H.; Murphy, C. J.; Gou, L. *Nano Lett.* **2004**, *4*, 1903–1907.

Published on Web 12/23/2010

effects on physical and chemical properties, recently, much effort has been devoted to the synthesis of Cu_2O micro/nanocrystals, such as octahedra,[16,17] nanocages,[18] nanocubes,[19] nanowires,[20] nanorods,[21] hollow nanostructures,[22] and other nanostructures.[23] Despite great advances in synthesizing Cu_2O nanomaterials with controlled nanostructures, until now, there have been almost no reports on Cu_2O nanotubes, and the preparation of Cu_2O nanotubes still represents a significant challenge in the field of nanoscale science. We believe Cu_2O nanotubes with a high surface area, high porosity, and excellent chemical stability are particularly attractive for the above-mentioned applications.

Herein, an electrodeposition−dissolution process accompanied by void generation was introduced for the synthesis of Cu_2O nanotubes. To the best of our knowledge, this is the first report on the preparation of single-crystalline hexagonal Cu_2O nanotubes. The basis of hollow tube formation is selective dissolution affecting the nanorod core preferentially, leaving lateral faces, resulting in a tubular structure. Although Cu_2O is metastable and less stable than CuO, we can easily control the formation of Cu_2O, and it is the only product in deposits. Our discovery may be of quite a general nature for the synthesis of nanotubes or hollow nanostructures and could be applied to many other dissoluble systems. The synthesis method reported here shows a simple and economical route for the preparation of Cu_2O nanotubes. These prepared hexagonal Cu_2O nanotube arrays were characterized by SEM, TEM, EDS, XRD, and XPS. Experimental results in this paper demonstrated that these prepared Cu_2O nanotubes had potential applications in gas sensors.

Experimental Section

A simple three-electrode cell was used in our experiments. A graphite electrode was used as a counter electrode (spectral grade, 1.8 cm^2). A saturated calomel electrode (SCE) was used as the reference electrode that was connected to the cell with a double salt bridge system. A pure Cu plate (99.99%, 1.0 cm^2) was used as a working electrode during the electrodeposition. All potential values determined in this study were the values vs SCE. The electrochemical deposition of Cu_2O was carried out in a solution of 0.003 M $Cu(NO_3)_2$ + 0.1 M NH_4Cl + 0.05 M KCl with a current density of 2.0 mA/cm^2 for 120 min at 70 °C by galvanostatic electrolysis. During the electrodeposition, Cu_2O nanorods are first deposited on the substrate, and then Cu_2O nanorods are dissolved in the same solution to form Cu_2O nanotubes under the role of NH_4Cl during electrodeposition. The obtained Cu_2O nanotubes were analyzed by X-ray diffraction (XRD, PIGAKU, D/MAX 2200 VPC) and an Oxford Instrument's INCA energy-dispersive spectrometer (EDS) to determine the chemical compositions and structures of deposits. The surface morphologies of these deposited films were observed by field emission scanning electron microscopy (FE-SEM, JSM-6330F), thermal field emission environment scanning electron microscopy (TFE-SEM, FEI, Quanta 400), and transmission electron microscopy (TEM, JEM-2010HR). X-ray photoelectron spectroscopy (XPS, ESCALAB 250) was used to assess the chemical state and surface composition of Cu_2O deposits. The measurement of photoluminescence spectra was carried out using a spectrofluorophotometer (RF-5301PC) at room temperature.

The gas sensing properties of Cu_2O nanotubes were investigated. The prepared Cu_2O was mixed with Terpineol and ground in an agate mortar to form a paste. The resulting paste was coated on a ceramic tube-like substrate on which a pair of Au electrodes had been printed previously, followed by drying at 100 °C for about 2 h and subsequent annealing at 600 °C for about 2 h. Finally, a small Ni−Cr alloy coil was inserted into the tube as a heater, which provided the working temperature of the gas sensor. The schematic drawing of the as-fabricated gas sensor is shown in Figure 6a. The response or recovery time was expressed as the time taken for the sensor output to reach 90% of its saturation after applying or switching off the gas in a step function.

Results and Discussion

The electrochemical deposition of Cu_2O nanotubes was carried out in a solution of 0.003 M $Cu(NO_3)_2$ + 0.1 M NH_4Cl+0.05 M KCl with a current density of 2.0 mA/cm^2 for 120 min at 70 °C. The electrochemical formation process of Cu_2O in this study can be suggested as follows. First, NO_3^- ions are electroreduced on the cathode surface, and then OH^- ions are produced.[24,25] Finally, these produced OH^- ions will react with Cu^+ ions that are electroreduced from Cu^{2+} ions to form Cu_2O. These processes are expressed as eqs 1 and 2.[26] The cyclic voltammogram of the Pt electrode in a solution of 0.003 M $Cu(NO_3)_2$ + 0.1 M NH_4Cl + 0.05 M KCl at 0.01 V/s is shown in Figure 1a. Two reduction waves are observed.

(16) (a) Kang, S.-O.; Hong, S.; Choi, J.; Kim, J.-S.; Hwang, I.; Byun, I.-S.; Kim, Y. S.; Kim, W.; Park, B. H. *J. Appl. Phys.* **2010**, *107*, 053704. (b) Cui, J.; Gibson, U. J. *J. Phys. Chem. C* **2010**, *114*, 6408–6412. (c) Radi, A.; Pradhan, D.; Sohn, Y.; Leung, K. T. *ACS Nano* **2010**, *4*, 1553–1560. (d) Sui, Y.; Fu, W.; Zeng, Y.; Yang, H.; Zhang, Y.; Chen, H.; Li, Y.; Li, M.; Zou, G. *Angew. Chem., Int. Ed.* **2010**, *49*, 4282–4285.
(17) (a) Siegfried, M. J.; Choi, K.-S. *Adv. Mater.* **2004**, *16*, 1743. (b) Guo, S.; Fang, Y.; Dong, S.; Wang, E. *Inorg. Chem.* **2007**, *46*, 9537–9539.
(18) (a) Jiao, S.; Xu, L.; Jiang, K.; Xu, D. *Adv. Mater.* **2006**, *18*, 1174–1746. (b) Lu, C.; Qi, L.; Yang, J.; Wang, X.; Zhang, D.; Xie, J.; Ma, J. *Adv. Mater.* **2005**, *17*, 2562–2567.
(19) (a) Gou, L.; Murphy, C. J. *Nano Lett.* **2003**, *3*, 231. (b) Siegfried, M. J.; Choi, K.-S. *J. Am. Chem. Soc.* **2006**, *128*, 10356–10357. (c) Liang, X.; Gao, L.; Yang, S.; Sun, J. *Adv. Mater.* **2009**, *21*, 1–4. (d) Liu, R.; Oba, F.; Bohannan, E. W.; Ernst, F.; Switzer, J. A. *Chem. Mater.* **2003**, *15*, 4882–4885.
(20) (a) Sahoo, S.; Husale, S.; Colwill, B.; Lu, T.-M.; Nayak, S.; Ajayan, P. M. *ACS Nano* **2009**, *3*, 3935–3944. (b) Wang, W.; Wang, G.; Wang, X.; Zhan, Y.; Liu, Y.; Zheng, C. *Adv. Mater.* **2002**, *14*, 67–69. (c) Orel, Z. C.; Anžlovar, A.; Dražić, G.; Žigon, M. *Cryst. Growth Des.* **2007**, *7*, 453–458.
(21) Ma, L.; Peng, M.; Li, J.; Yu, Y.; Chen, Z. *IEEE-NANO 2007, 7th IEEE Conference 2007*; IEEE: Los Alamitos, CA, 2007; pp 975−978.
(22) (a) Park, J. C.; Kim, J.; Kwon, H.; Song, H. *Adv. Mater.* **2009**, *21*, 803–807. (b) Xu, H.; Wang, W. *Angew. Chem., Int. Ed.* **2007**, *46*, 1489–1492. (c) Gao, J.; Li, Q.; Zhao, H.; Li, L.; Liu, C.; Gong, Q.; Qi, L. *Chem. Mater.* **2008**, *20*, 6263–6269. (d) Firmansyah, D. A.; Kim, T.; Kim, S.; Sullivan, K.; Zachariah, M. R.; Lee, D. *Langmuir* **2009**, *25*, 7063–7071. (e) Hung, L.-I.; Tsung, C.-K.; Huang, W.; Yang, P. *Adv. Mater.* **2010**, DOI: 10.1002/adma.200903947.
(23) (a) Siegfried, M. J.; Choi, K.-S. *Angew. Chem., Int. Ed.* **2005**, *44*, 3218–3223. (b) Siegfried, M. J.; Choi, K.-S. *Angew. Chem., Int. Ed.* **2007**, *47*, 368–372. (c) Miyake, M.; Chen, Y.-C.; Braun, P. V.; Wiltzius, P. *Adv. Mater.* **2009**, *21*, 3012–3015. (d) Nachimuthu, P.; Thevuthasan, S.; Kim, Y. J.; Lea, A. S.; Shutthanandan, V.; Engelhard, M. H.; Baer, D. R.; Chambers, S. A.; Shuh, D. K.; Lindle, D. W.; Gullikson, E. M.; Perera, R. C. C. *Chem. Mater.* **2003**, *15*, 3939–3946.
(24) (a) Fu, M.; Zhou, J.; Xiao, Q.; Li, B.; Zong, R.; Chen, W.; Zhang, J. *Adv. Mater.* **2006**, *18*, 1001–1004. (b) Pradhan, D.; Tong Leung, K. *Langmuir* **2008**, *24*, 9707–9716. (c) Elias, J.; Tena-Zaera, R.; Lévy-Clément, C. *J. Phys. Chem. C* **2008**, *112*, 5736–5741. (d) Xu, L.; Chen, Q.; Xu, D. *J. Phys. Chem. C* **2007**, *111*, 11560–11565.
(25) (a) Li, L.; Pan, S.; Dou, X; Zhu, Y.; Huang, X.; Yang, Y.; Li, G.; Zhang, L. *J. Phys. Chem. C* **2007**, *111*, 7288. (b) Lin, C.; Lin, H.; Li, J.; Li, X. *J. Alloys Compd.* **2008**, *462*, 175–180. (c) Rudolph, M.; Loewenstein, T.; Arndt, E.; Zimmermann, Y.; Neudeck, A.; Schlettwein, D. *Phys. Chem. Chem. Phys.* **2009**, *11*, 3313–3319.
(26) Lee, Y.-H.; Leub, I.-C.; Liao, C.-L.; Fung, K.-Z. *J. Alloys Compd.* **2007**, *436*, 241–246.

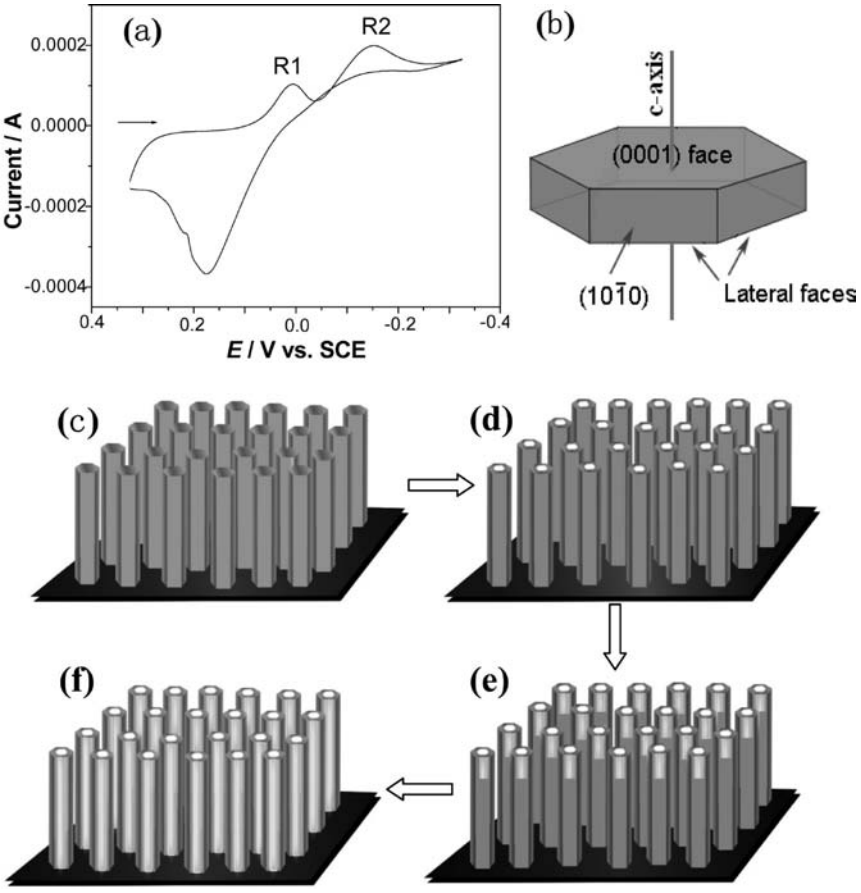

Figure 1. (a) Cyclic voltammogram of 0.003 M $Cu(NO_3)_2$ + 0.1 M NH_4Cl + 0.05 M KCl solution at 0.01 V/s. (b) Crystal faces in hexagonal Cu_2O. Schematic illustration of Cu_2O nanorod dissolution process accompanied by hollow generation that is applied to the synthesis of Cu_2O nanotube arrays. (c) A Cu_2O nanorod array is used for the starting precursor. (d) The dissolution process happens at the top surface of Cu_2O nanorods. (e) Formation of partial hollow Cu_2O nanorods. (f) Formation of hollow Cu_2O nanotubes.

The wave R1 corresponds to reaction 1, and the wave R2 corresponds to reaction 2.

$$NO_3^- + H_2O + 2e^- \rightarrow NO_2^- + 2OH^- \quad (1)$$

$$2Cu^{2+} + 2e^- + 2OH^- \rightarrow Cu_2O + H_2O \quad (2)$$

Herein, our design strategy for the synthesis of Cu_2O nanotubes is based on a two-step solution approach, which involves the electrodeposition of the oriented Cu_2O nanorods and a synchronously selective dissolution process accompanied by void generation, and is schematically displayed in Figure 1c−f. Cu_2O nanorod arrays are firstly electrodeposited and are employed as the precursors. To realize the dissolution process of Cu_2O nanorods, NH_4Cl as an additive is added into the deposition solution. The dissolution mechanism of Cu_2O deposits can be explained as follows. During electrodeposition, NH_4^+ ions in solution can react with the produced OH^- ions to form NH_3 (reaction 3). Then, the produced NH_3 will react with Cu_2O to form a copper(II)−amine complex (reaction 4), which is soluble in a water solution. Therefore, NH_4^+ ions in solution are crucial for the dissolution of Cu_2O. A large number of Cl^- ions accompanied with NH_4^+ ions are also added into the deposition solution, and they will be adsorbed on the surface of Cu_2O nanorods. In addition, Cl^- ions in solution will also lead to the formation of $CuCl_4^{2-}$ ions in a deposition solution via reaction 5.[27] These formed $CuCl_4^{2-}$ ions will also be adsorbed on the surfaces of Cu_2O nanorods because of the electrostatic adherence. These adsorbed Cl^- and $CuCl_4^{2-}$ ions may provide the electrons to Cu^+ in Cu_2O, change the charge distribution between Cu^+ and O^{2-}, and enhance Cu−O bond. The chemical effect by the specific adsorption of Cl^- and $CuCl_4^{2-}$ ions will lead to the dissolution rate of Cu_2O on the surface of nanorods being much slower than that in the nanorod inner section. So the selective dissolution affects the center part of the Cu_2O nanorod preferentially along the *c* axis, leaving the lateral faces and resulting in a tubular structure as shown in Figure 1f. The crystal faces in hexagonal Cu_2O are shown in Figure 1b.

$$NH_4^+ + OH^- \rightarrow NH_3 + H_2O \quad (3)$$

$$Cu_2O + \frac{1}{2}O_2 + 2H_2O + 8NH_3 \rightarrow 2[Cu(NH_3)_4]^{2+} + 4OH^- \quad (4)$$

$$4Cl^- + Cu^{2+} \rightarrow CuCl_4^{2-} \quad (5)$$

Figure 2a shows that high-density hexagonal Cu_2O nanotube arrays were successfully synthesized on a large area of

(27) (a) Vancoillie, S.; Pierloot, K. *J. Phys. Chem. A* **2008**, *112*, 4011–4019. (b) Earl, B. L. *J. Chem. Educ.* **1985**, *62*, 798.

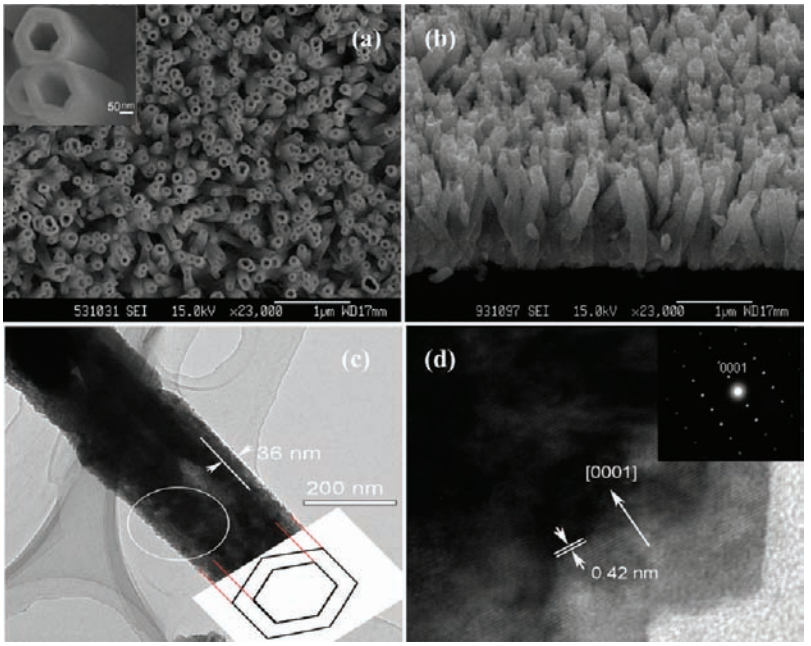

Figure 2. SEM images of Cu_2O nanotubes electrodeposited in a solution of 0.003 M $Cu(NO_3)_2$ + 0.1 M NH_4Cl + 0.05 M KCl for 120 min at 70 °C with a current density of 2.0 mA/cm^2. (a) Top view. (b) Side view. (c) TEM image. (d) HRTEM image and SAED pattern (the inset).

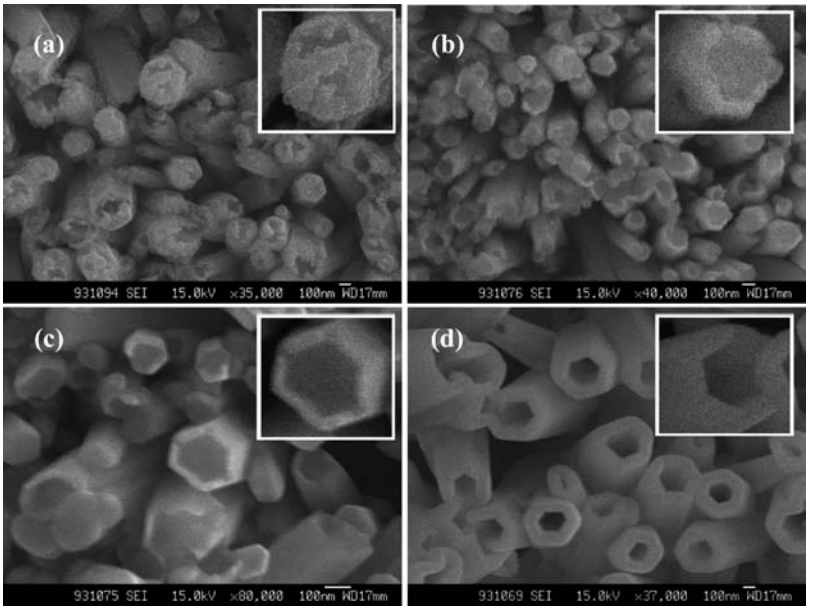

Figure 3. SEM images of the Cu_2O deposits in various stages during the growth. The evolvement sequence is a → b → c → d.

the substrate. The average diameter of these Cu_2O nanotubes is about 250 nm, and the average thickness of their walls is about 50 nm. A SEM image of the side view of the Cu_2O nanotube arrays is shown in Figure 2b, which shows that the average length of these Cu_2O nanotubes is about 1 μm. Figure 2c shows a TEM image of the Cu_2O nanotube. The diameter of this nanotube is about 260 nm, and its wall thickness is about 36 nm. The HRTEM image of the Cu_2O nanotube is shown in Figure 2d, which clearly shows that the lattice fringes are derived from the same crystalline grains. The lattice spacing is estimated from the HRTEM image, and it is about 0.42 nm, which corresponds to a (0001) planar spacing of Cu_2O. So the crystal growth of the nanotubes is preferential in the [0001] direction. These prepared Cu_2O nanotubes were further characterized by selected-area electron diffraction (SAED). The SAED pattern is shown in the inset in Figure 2d, and it also shows that the prepared Cu_2O nanotube consists of single crystal structures with preferential growth in the [0001] direction. Therefore, the uniform single crystal Cu_2O nanotubes were successfully synthesized.

In order to demonstrate the formation mechanism of Cu_2O nanotubes displayed in Figure 1, SEM images of the deposits in various growth stages were characterized as shown in Figure 3. In the early stages, the partial dissolution of the core just happens at the tip of the Cu_2O nanorods, as shown in Figure 3a. The depth of the hollow structure increased with time, as shown in Figure 3b and c, and finally the Cu_2O nanotubes were obtained as shown in Figure 3d. According

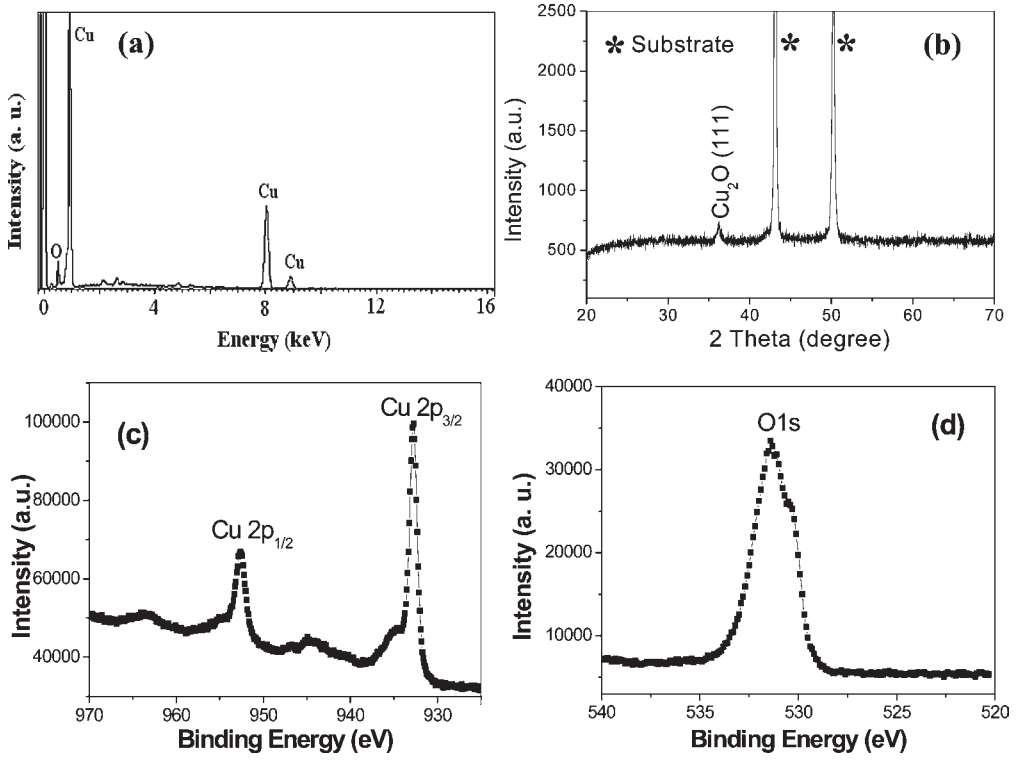

Figure 4. (a) EDS and (b) XRD patterns of Cu_2O nanotubes. XPS spectra of Cu_2O nanotubes: (c) Cu 2p and (d) O 1s.

to the above experimental observations, the evolution of the dissolution process is accordant with the schematics shown in Figure 1.

EDS measurement was carried out at a number of locations throughout the deposits to confirm the composition of Cu_2O. The EDS pattern is shown in Figure 4a, and it reveals that the elements of O and Cu exist in the obtained deposits. The composition analysis by EDS reveals that the Cu/O ratio is about 2:1. The typical XRD pattern of the as-prepared Cu_2O nanotubes is shown in Figure 4b, and it identifies the product as Cu_2O (JCPDS No. 05-0667). No impurities such as cupric oxides are found in the XRD pattern besides the substrate. XPS analysis was also conducted in order to further confirm the chemical bonding properties and phase of the deposit. The XPS spectrum from 970 to 925 eV shown in Figure 4c demonstrats the photoelectron spectrum of the Cu 2p core level for the deposit. The binding energies obtained in XPS analysis were corrected for specimen charging by referencing the C 1s to 284.60 eV. Compared with the binding energy of Cu 2p 3/2, the peak located at 932.4 eV can be attributed to Cu^+ species as reported previously.[28] The O 1s spectrum for the surface of the sample is shown in Figure 4d. The peak at 530.5 eV corresponds to O^{2-} ions in Cu_2O. The peak at 531.2 eV can be attributed to absorbed H_2O or O_2 onto the surface.[29] Therefore, the results of EDS, XRD, and XPS all prove that Cu_2O is the only product, and they all exclude the existence of CuO in the deposits.

Since bulk Cu_2O is a luminescent material, the photoluminescence (PL) properties of these prepared Cu_2O nanotubes were tested. The PL spectrum of the prepared Cu_2O nanotubes is shown in Figure 5. The luminescent peak at 491 nm may be attributed to the band edge emission from Γ_1^+ to the new sublevels at 298 K.[30] The luminescent peak at 503 nm may be attributed to the imperfection levels as a result of the interaction of two excitons or the $^3D-^1D$ splitting in Cu^+ ($3d^94s^2$).[31] In addition, luminescent peaks at 436, 466, and 522 nm were also observed, and they may be attributed to defects in Cu_2O nanotubes.[32] The peak at 436 nm shows a high intensity, indicating a strong emission. This suggests there is a greater fraction of copper or oxygen vacancies in the prepared Cu_2O nanotubes.

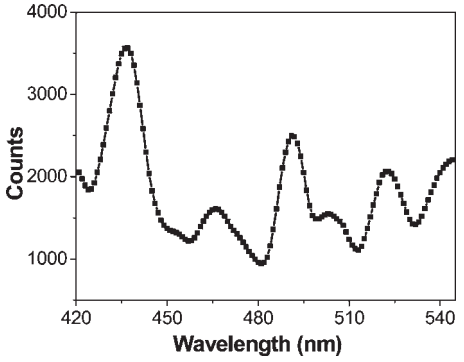

Figure 5. Photoluminescence spectrum of the prepared Cu_2O nanotubes.

(28) Shang, W.; Shi, X.; Zhang, X.; Ma, C.; Wang, C. *Appl. Phys. A: Mater. Sci. Proc.* **2007**, *87*, 129–135.
(29) Szörényi, T.; Laude, L. D.; Bertóti, I.; Kántor, Z.; Geretovszky, Z. *J. Appl. Phys.* **1995**, *78*, 6211.
(30) Rossetti, R.; Ellison, L.; Gibson, J. M.; Brus, L. E. *J. Chem. Phys.* **1984**, *80*, 4464–4469.
(31) Elliott, R. J. *Phys. Rev.* **1961**, *124*, 340–345.
(32) Yang, Z.; Chiang, C.-K.; Chang, H.-T. *Nanotechnology* **2008**, *19*, 025604:1–025604:7.
(33) Gutierrez-Sosa, G. A.; Baraldi, A.; Larciprete, R.; Lizzit, S. *J. Am. Chem. Soc.* **2002**, *124*, 7117–7122.
(34) Zhang, Y.; Xu, J.; Xiang, Q.; Li, H.; Pan, Q; Xu, P. *J. Phys. Chem. C* **2009**, *113*, 3430–3435.

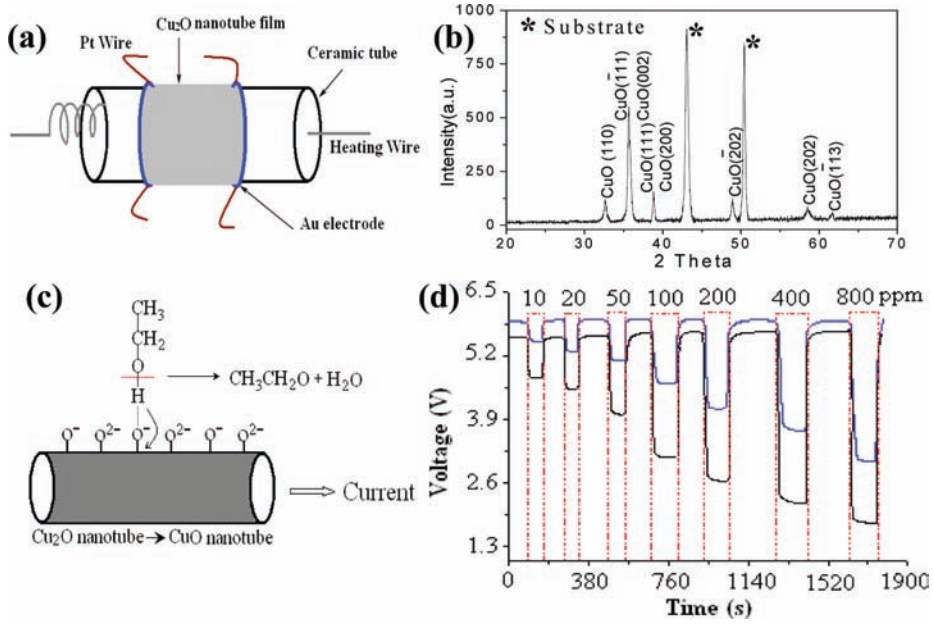

Figure 6. (a) Schematic diagram of the structure of a typical Cu_2O nanotube gas sensor. (b) XRD pattern of CuO nanotube arrays. (c) Schematic representation of the mechanism of reaction of the CuO nanotube sensor to ethanol. (d) Typical response curves of CuO nanotube sensor (black curve) and CuO nanorod sensor (blue curve) to alcohol with increasing concentration at 210 °C.

The alcohol gas sensor application of CuO nanotube arrays is investigated in this paper via the conversion of Cu_2O nanotube arrays to CuO nanotube arrays. As Cu_2O is metastable and the analyte gas, C_2H_5OH, needs to be injected into a test chamber and mixed with air at 210 °C, these prepared Cu_2O nanotube arrays will be changed to CuO nanotube arrays. Recently, CuO nanomaterials have attracted much interest for use in gas sensor applications.[35,36] Before measurements, the prepared Cu_2O nanotube arrays were first mixed with Terpineol and ground in an agate mortar to form a paste. The resulting paste was coated on a ceramic tube-like substrate, followed by drying at 100 °C for about 2 h and subsequent annealing at 600 °C for about 2 h. The isothermal response curves were measured in ambient air with increasing alcohol concentrations of 10−800 ppm at 210 °C. Under the above conditions, the Cu_2O nanotube arrays were accordingly converted to CuO nanotube arrays via reaction 6, and the XRD pattern is shown in Figure 6b, which proves the existence of CuO nanotube arrays.

$$2Cu_2O + O_2 \rightarrow 4CuO \qquad (6)$$

The electrical conductivity in CuO nanotubes can be well modulated by the adsorbed gas molecules. The sensing mechanism of CuO is illustrated in Figure 6c. In the sensors based on CuO nanotube arrays, a large amount of negative charged oxygen (O^-, O^{2-}) will be absorbed on the outer or inner surfaces of nanotubes, and the surface properties become paramount. When in contact with the reducing gas, such as alcohol, the negative charged oxygen (O^-, O^{2-}) will react with it through hydrogen bonds to change the conductivity of the sensors. Detecting gas C_2H_5OH was injected into a test chamber and mixed with air. The gas response of the sensor in this paper is defined as $S = R_a/R_g$, where R_a and R_g are the resistances in air and test gas, respectively. The resistance of a sensor in air or test gas was measured by monitoring voltage. It is clear that the nanotube arrays in the film can provide enough surface area and interspaces to contact the detected gas. Figure 6d shows a typical isothermal response curve of the CuO nanotube array sensor when cycled by increasing alcohol concentrations in ambient air with a range of 10−800 ppm at 210 °C (black curve). According to the above result, it is obvious that the CuO nanotube array sensor has a very high response to ethanol, showing promise as an ethanol-sensing material. All of the response times of the CuO nanotube array sensors in alcohol of concentrations in the range of 10−800 ppm are about 12 s, and the recovery times are about 22 s. The typical isothermal response curve of CuO nanorods is shown in Figure 6d (blue curve). Compared with CuO nanotube arrays, CuO nanorods show a relatively weak ethanol sensing response. Therefore, the CuO nanotube array sensor offers a quick response/recovery time compared with that reported for CuO or ZnO in the literature.[35−38] The high gas sensing response of the CuO nanotube arrays can be attributed to the large surface area and high porosity of nanotubes and more active centers that are obtained from the enhanced oxygen vacancy defects. Moreover, the CuO nanotube arrays could increase the number of the gas channels leading to more effective surface areas (defined as the areas which can contact the gas). Considering the selectivity of the CuO nanotube array sensor, we have detected H_2S gas with the same concentration level at a working temperature of 210 °C, and we find it is not sensitive enough for practical usage and the voltage response is not proportional to the increasing concentration of H_2S.

(35) Wang, C.; Fu, Q. X.; Xue, X .Y.; Wang, Y. G.; Wang, T. H. *Nanotechnology* **2007**, *18*, 145506.
(36) Raksa, P.; Gardchareon, A.; Chairuangsri, T.; Mangkorntong, P.; Mangkorntong, N.; Choopun, S. *Ceram. Int*. **2009**, *35*, 649–652.
(37) Hsueh, T.-J.; Chang, S.-J.; Hsu, C.-L.; Lin, Y.-R.; Chen, I.-C. *J. Electrochem. Soc*. **2008**, *155*, K152–K155.
(38) Wan, Q.; Li, Q. H.; Chen, Y. J.; Wang, T. H.; He, X. L.; Li, J. P.; Lin, C. L. *Appl. Phys. Lett*. **2004**, *84*, 3654–3656.

Conclusions

In summary, an electrodeposition−dissolution process accompanied by void generation has been investigated for the synthesis of Cu_2O nanotube arrays. Herein, NH_4Cl was found to be an effectual additive, and it can successfully realize the dissolution process of Cu_2O from nanorods to nanotubes. The gas sensing measurements show that the prepared Cu_2O nanotube arrays have potential applications in gas sensors by converting to CuO nanotube arrays, which may be attributed to nanotube structures with a large surface area and high porosity and more active centers that are obtained from the enhanced oxygen vacancy defects. It is believed that this synthesis route can be applied to many materials that can be grown by electrodeposition techniques, including compound material nanotubes. Further research work is underway to formulate the details of the growth and have better control of the wall thickness of the nanotube by understanding its dependence on the dissolution process.

Acknowledgment. This work was supported by NSFC (21073240, 20603048, 20873184, and 90923008), Guangdong Province (2008B010600040 and 9251027501000002), and the Fundamental Research Funds for the Central Universities (09lgpy17). We all thank Dr. P. Wang for help in gas sensor measurements at UCR.